Available online at www.sciencedirect.com
ScienceDirect
Nuclear Physics A 818 (2009) 152–173
NUCLEAR PHYSICS A
www.elsevier.com/locate/nuclphysa

Similarity renormalization group evolution of many-body forces in a one-dimensional model

E.D. Jurgenson, R.J. Furnstahl *

Department of Physics, The Ohio State University, Columbus, OH 43210, USA

Received 28 October 2008; received in revised form 22 December 2008; accepted 22 December 2008

Available online 25 December 2008

Abstract

A one-dimensional system of bosons with short-range repulsion and mid-range attraction is used as a laboratory to explore the evolution of many-body forces by the Similarity Renormalization Group (SRG). The free-space SRG is implemented for few-body systems in a symmetrized harmonic oscillator basis using a recursive construction analogous to no-core shell model implementations. This approach, which can be directly generalized to three-dimensional nuclei, is fully unitary up to induced A-body forces when applied with an A-particle basis (e.g., A-body bound-state energies are exactly preserved). The oscillator matrix elements for a given A can then be used in larger systems. Errors from omitted induced many-body forces show a hierarchy of decreasing contribution to binding energies. An analysis of individual contributions to the growth of many-body forces demonstrates such a hierarchy and provides an understanding of its origins.

PACS: 21.30.-x; 05.10.Cc; 13.75.Cs

Keywords: Renormalization group; Flow equations; Nuclear forces

1. Introduction

A major goal of nuclear structure theory is to make quantitative calculations of nuclear observables starting from microscopic internucleon forces. The Similarity Renormalization Group (SRG) [1–3], through a continuous series of unitary transformations that soften initial interactions, can dramatically reduce the computational requirements of low-energy many-body calculations [4–6]. At the same time, the SRG induces many-body forces as it evolves the Hamiltonian.

* Corresponding author.
E-mail addresses: jurgenson.1@osu.edu (E.D. Jurgenson), furnstahl.1@osu.edu (R.J. Furnstahl).

0375-9474/$ – see front matter
doi:10.1016/j.nuclphysa.2008.12.007

For the SRG to be a useful tool, we must develop methods for calculating these many-body interactions and establish the conditions under which an initial hierarchy of many-body forces is maintained. In this paper, we study one-dimensional systems of bosons as a proof-of-principle of a practical method to evolve and evaluate such forces, and establish a road map for full three-dimensional calculations.

The SRG can be implemented as a flow equation for the evolving Hamiltonian H_s,

$$\frac{dH_s}{ds} = [\eta_s, H_s] = \big[[G_s, H_s], H_s\big]. \tag{1}$$

Here s is a flow parameter and the flow operator G_s specifies the type of SRG [4,7]. Most previous applications to nuclear structure have been in a momentum basis, where decoupling between low-energy and high-energy matrix elements is naturally achieved by choosing a momentum-diagonal flow operator such as the kinetic energy $T_{\rm rel}$. However we can evaluate Eq. (1) with $G_s = T_{\rm rel}$ in any convenient basis.

In Ref. [8], a diagrammatic approach to the SRG equation was introduced, which organized the independent evolution of two- and three-body (and higher-body) potentials. This formalism is necessary in a momentum basis to avoid "dangerous" delta functions from spectator particles. An alternative is to work in a discrete basis for which Eq. (1) can be applied directly in each n-body sector without a separate evolution for few-body forces; that is, the Hamiltonian is evolved as a whole. We adopt this approach in the present work, using harmonic oscillator wave functions as our basis and mimicking the formalism used in the no-core shell model (NCSM) [9–11] to create properly symmetrized (for bosons) matrix elements in relative (Jacobi) coordinates. The restriction to one dimension makes the construction particularly straightforward and requires only moderate matrix sizes. We use bosons in this paper for easy comparison with existing model analysis. The boson ground states coincide with fermion ground states when the flavor degeneracy is greater than the number of particles, because the overall anti-symmetrization is realized by the flavor wave function.

We use simple flavor-independent potentials that imitate the short-range repulsion and mid-range attraction characteristic of realistic local nuclear potentials. Previous studies of the SRG imply that properties of the transformations are primarily due to the matrix structure (G_s, H_s, choice of basis, etc.), so we expect to be able to directly carry over at least some of our observations to three dimensions. Because the NCSM formalism is already developed, the generalization to three-dimensional fermionic calculations with spin–isospin degrees of freedom and using realistic nuclear interactions should be algebraically straightforward (although far more computationally intensive).

The plan of the paper is as follows. In Section 2, we develop the one-dimensional version of the oscillator basis techniques. These include building symmetrizer operators to construct symmetric basis states of bosons and fermions, embedding potential and kinetic energy operators in a given oscillator basis, and developing a scheme to organize the oscillator basis states in a universal and scalable manner. In Section 3, results are given for two- through five-particle systems. The two-particle calculations establish that the models simulate the relevant features of previous nuclear calculations [4–6,12]. Then three- and higher-particle calculations are used to explore the running of the few-body potentials. Section 4 summarizes our observations and conclusions.

2. Formalism

In this section, we adapt to one dimension the recursive symmetrization formalism developed by Navratil and collaborators for use in NCSM calculations with a translationally invariant har-

monic oscillator basis [9–11]. While the three-dimensional formalism is well documented, the one-dimensional analog is not, so we provide a self-contained treatment here.

2.1. Jacobi coordinates

The initial (i.e., unevolved) one-dimensional Hamiltonian for A bosons of equal mass m with a local two-body potential has the first-quantized form (in units with $\hbar = 1$)

$$H = \frac{1}{2m}\sum_{i=1}^{A} k_i^2 + \sum_{i<j=1}^{A} V(x_i - x_j), \tag{2}$$

where the x_i are single-particle coordinates and the k_i are single-particle momenta. To connect to the nuclear problem of interest that uses potentials given in a momentum basis (e.g., chiral effective field theory potentials), we calculate matrix elements using harmonic oscillator basis states in Jacobi momentum coordinates. This representation also provides a clean visual interpretation of the SRG evolution of potentials.

With equal-mass particles, a convenient set of relative momentum Jacobi coordinates is defined by (for $j = 1$ to $A - 1$)

$$p_j = \sqrt{\frac{j}{j+1}}\left(\frac{1}{j}\sum_{i=1}^{j} k_i - k_{j+1}\right), \tag{3}$$

where the k_i are the single-particle momenta of the A particles. Sometimes for convenience we will use $p \equiv p_1$ and $q \equiv p_2$ when restricted to $A \leqslant 3$. We define the Fourier transform $V(x_1 - x_2)$ to $V(p_1, p_1')$ as

$$V(p_1, p_1') = \int V(\sqrt{2}\ell_1) e^{-i(p_1 - p_1')\ell_1}\, d\ell_1, \tag{4}$$

where $\ell_1 = (x_1 - x_2)/\sqrt{2}$ is the coordinate conjugate to the Jacobi momentum p_1. We introduce a set of harmonic oscillator states $|n_j\rangle$ corresponding to each of the coordinates of Eq. (3), so a general product basis state has the form

$$\prod_{j=1}^{A-1} \langle p_j | n_j \rangle, \tag{5}$$

with $n_j = 0, 1, 2, \ldots, N_{\max}$ for each j. In the next section we discuss how to build linear combinations of these states that have the appropriate symmetry.

2.2. Symmetrization

We carry out the SRG evolution for each A-particle subsystem in a complete basis of properly symmetrized states, which will be linear combinations of the basis states of Eq. (5). The symmetrization procedure is adapted from the procedure developed for NCSM calculations [9–11]. This entails symmetrizing first the two-particle system and then using a recursive procedure to go from the $(A - 1)$-particle basis to an A-particle basis. At each stage we keep only symmetric states, identified as eigenstates of the symmetrizer with eigenvalue unity.

The two-particle system is specified by the oscillator number n_1. The symmetrizer is $(1 + P_{12})/2$, where P_{ij} is the exchange operator between particles i and j. Because $P_{12}|n_1\rangle =$

$(-1)^{n_1}|n_1\rangle$, the symmetrizer in the two-particle case has eigenvalue one acting on states with n_1 even and zero when acting on states with n_1 odd. Thus the symmetric basis states have n_1 even and we simply omit the odd states. Following conventions from Ref. [9], we label these eigenstates as $|N_2 i_2\rangle$, where N_2 is the total oscillator number of the symmetric state and i_2 is an arbitrary label which distinguishes states degenerate in N_2. In the two-particle case the notation is trivial, with $N_2 = n_1$ even and $i_2 = 1$. We write eigenstate projection coefficients as $\langle N_2 i_2 \| n_1\rangle = \delta_{N_2,n_1}(1 + (-1)^{n_1})/2$. These are referred to in the literature as the "coefficients of fractional parentage".

A three-particle basis is specified by product states of the two-body symmetric eigenstates, $|N_2 i_2\rangle$, and single-particle states with the oscillator number corresponding to the third particle, $|n_2\rangle$. The symmetrizer for this system is governed by the permutation group, S_3, which can be defined by just two of its generators. Here we choose the permutation operators P_{12} and P_{23}. The symmetrization operator can be written as

$$S = \frac{1}{6}(1 + P_{12} + P_{23} + P_{12}P_{23} + P_{23}P_{12} + P_{12}P_{23}P_{12}). \tag{6}$$

We build this symmetrizer in the basis $|N_2 i_2; n_2\rangle \equiv |N_2 i_2\rangle|n_2\rangle$ where the states $|N_2 i_2\rangle$ are already eigenstates of P_{12} with eigenvalue one, so Eq. (6) reduces to $S = (1 + 2P_{23})/3$.

In this basis, the matrix elements of P_{23} can be expressed as

$$\langle N_2' i_2'; n_2'|P_{23}|N_2 i_2; n_2\rangle = \delta_{N',N}\langle n_1' n_2'|n_1 n_2\rangle_3, \tag{7}$$

where $N \equiv N_2 + n_2 = N_2' + n_2' = N'$ and $\langle n_1' n_2'|n_1 n_2\rangle_3$ is the one-dimensional harmonic oscillator transformation bracket for particles with mass ratio 3. We construct these transformation brackets and generalize to mass ratio d in Appendix A. By diagonalizing this symmetrizer we identify the symmetric eigenstates of the system as the ones with eigenvalue unity. We keep only those states and discard the others. This set of eigenvectors gives us the coefficients of fractional parentage, $\langle N_2 i_2; n_2 \| N_3 i_3\rangle$, of the three-boson symmetric eigenstates, $|N_3 i_3\rangle$, in terms of the original partially symmetrized three-particle space, $|N_2 i_2; n_2\rangle$. Note that i_3 is not trivial like i_2, because in the three-body system there are eigenstates degenerate in the total oscillator number, $N_2 + n_2$. The label i_3 keeps track of those degeneracies. We find in the one-dimensional system of bosons that the fraction of symmetric basis states for $A = 3$ is about one-fifth. For $A = 4$ the reduction in number of states is above 90%.

To construct the basis states for higher A, we generalize this procedure. To go from $A - 1$ to A we need only to symmetrize between the last two particles, so we construct the symmetrizer

$$S_A = \frac{1}{A}\big(1 + (A-1)P_{(A-1)A}\big) \tag{8}$$

in the space of $(A-1)$-particle symmetric eigenstates and the additional Jacobi state, n_{A-1}. We label the basis of this space as $|N_{A-1} i_{A-1}; n_{A-1}\rangle$. The matrix element of the exchange operator in this space is

$$\begin{aligned}
&\langle N'_{A-1} i'_{A-1}; n'_{A-1}|P_{(A-1)A}|N_{A-1} i_{A-1}; n_{A-1}\rangle \\
&\quad = \delta_{N'_{A-1}+n'_{A-1},N_{A-1}+n_{A-1}} \sum \langle N'_{A-1} i'_{A-1} \| N_{A-2} i_{A-2}; n'_{A-2}\rangle \\
&\qquad \times \langle N_{A-2} i_{A-2}; n_{A-2} \| N_{A-1} i_{A-1}\rangle \langle n'_{A-2} n'_{A-1}|n_{A-2} n_{A-1}\rangle_{A(A-2)},
\end{aligned} \tag{9}$$

where the sum is over N_{A-2}, i_{A-2}, n_{A-2} and n'_{A-2}. The only significant difference from the three-particle case is that we must sum over the components of the $A - 1$ subcluster symmetric

states to get all the contributions to the exchange of the last two bosons, n_{A-2} and n_{A-1}. The parameter $d = A(A-2)$ can be derived by taking the last two Jacobi coordinates p_{A-2} and p_{A-1}, as defined in Eq. (3), and finding the transformation that exchanges particles labeled by k_{A-1} and k_A. This procedure is shown in Appendix A

For fermions, we need a complete basis of fully anti-symmetrized states. If we consider the one-flavor case, the procedure for our one-dimensional model is a trivial modification of Eqs. (6) and (8), namely all odd permutations come with a minus sign. Thus, for $A = 3$ the anti-symmetrizer can be written

$$A = \frac{1}{3}(1 - 2P_{23}), \tag{10}$$

where P_{23} acts on the flavor space as well. If there are more flavors than particles and the interaction is flavor independent, the spatial wave function for the ground state will be symmetric and correspond to our boson ground state wave functions. For realistic three-dimensional nuclei, the required construction of an anti-symmetric Jacobi basis with full angular momentum coupling has been worked out for the NCSM by Navratil et al. [9–11].

2.3. Hamiltonian matrix elements

To obtain the Hamiltonian in the symmetric eigenbasis of the general A-particle system, we employ a recursive embedding procedure that utilizes the partially symmetric bases developed for the symmetrization operator. First we treat the kinetic energy and then the potential.

The relative kinetic energy in the three-particle system is the total minus the center-of-mass kinetic energies:

$$\begin{aligned} T_{\text{rel}} &\equiv T_{\text{tot}} - T_{\text{cm}} \\ &= \frac{k_1^2}{2m} + \frac{k_2^2}{2m} + \frac{k_3^2}{2m} - \frac{(k_1+k_2+k_3)^2}{2(3m)} \\ &= \frac{p_1^2 + p_2^2}{2m}, \end{aligned} \tag{11}$$

where the p_i's are defined in Eq. (3). Momentum basis states are organized by increasing kinetic energy. We can project T_{rel} directly onto the three-particle oscillator basis by using the ladder operator definitions of the Jacobi momenta. The projection of T_{rel} into the $|n_1 n_2\rangle$ basis is

$$\begin{aligned} \langle n_1' n_2' | T_{\text{rel}} | n_1 n_2 \rangle &= \langle n_1' n_2' | \frac{p_1^2 + p_2^2}{2m} | n_1 n_2 \rangle \\ &= \frac{1}{2m} \frac{-m\omega}{2} \langle n_1' n_2' | \left(\eta_1^\dagger - \eta_1\right)^2 + \left(\eta_2^\dagger - \eta_2\right)^2 | n_1 n_2 \rangle, \end{aligned} \tag{12}$$

where the η_1 and η_2 operators act on the n_1 and n_2 spaces, respectively. Continuing, we get

$$\begin{aligned} \langle n_1' n_2' | T_{\text{rel}} | n_1 n_2 \rangle &= \frac{1}{2m} \frac{-m\omega}{2} \left[\langle n_1' | \left(\eta_1^\dagger - \eta_1\right)^2 | n_1 \rangle \delta_{n_2, n_2'} + \langle n_2' | \left(\eta_2^\dagger - \eta_2\right)^2 | n_2 \rangle \delta_{n_1, n_1'} \right] \\ &= \frac{-\omega}{4} \Big[\Big(\sqrt{(n_1+1)(n_1+2)}\, \delta_{n_1', n_1+2} + \sqrt{n_1(n_1-1)}\, \delta_{n_1', n_1-2} \\ &\quad - (2n_1+1)\delta_{n_1', n_1} \Big) \delta_{n_2', n_2} \\ &\quad + \Big(\sqrt{(n_2+1)(n_2+2)}\, \delta_{n_2', n_2+2} + \sqrt{n_2(n_2-1)}\, \delta_{n_2', n_2-2} \\ &\quad - (2n_2+1)\delta_{n_2', n_2} \Big) \delta_{n_1', n_1} \Big]. \end{aligned} \tag{13}$$

As noted, we keep only the n_1-even states using the projector $\langle N_2 i_2 \| n_1 \rangle$, and we can symmetrize the full three-particle system with the symmetric eigenstates, $|N_3 i_3\rangle$ whose components are given by $\langle N_3 i_3 \| N_2 i_2; n_2 \rangle$.

To derive the A-body kinetic energy in the symmetrized basis, $(T_A)_{\rm sym}$, we use a recursive procedure on the $(A-1)$-body result to find the A-particle space operator matrix elements:

$$
\begin{aligned}
(T_A)_{\rm sym} &= \langle N'_A i'_A | T_A | N_A i_A \rangle \equiv \langle N'_A i'_A | \sum_{i=1}^{A-1} p_i^2/2m | N_A i_A \rangle \\
&= \langle N'_A \| N'_{A-1} n'_{A-1} \rangle \langle N'_{A-1} n'_{A-1} | T_A | N_{A-1} n_{A-1} \rangle \langle N_{A-1} n_{A-1} \| N_A \rangle \\
&= \langle N'_A \| N'_{A-1} n'_{A-1} \rangle \big[\langle N'_{A-1} n'_{A-1} | (T_{A-1})_{\rm sym} + p_{A-1}^2/2m | N_{A-1} n_{A-1} \rangle \big] \\
&\quad \times \langle N_{A-1} n_{A-1} \| N_A \rangle \\
&= \langle N'_A \| N'_{A-1} n'_{A-1} \rangle \big[\langle N'_{A-1} | (T_{A-1})_{\rm sym} | N_{A-1} \rangle \delta_{n'_{A-1}, n_{A-1}} \\
&\quad + \delta_{N'_{A-1}, N_{A-1}} \langle n'_{A-1} | p_{A-1}^2/2m | n_{A-1} \rangle \big] \langle N_{A-1} n_{A-1} \| N_A \rangle \\
&= \langle N'_A \| N'_{A-1} n'_{A-1} \rangle \bigg[(T_{A-1})_{\rm sym} \delta_{n'_{A-1}, n_{A-1}} - \frac{\omega}{4} \delta_{N'_{A-1}, N_{A-1}} \big(\delta_{n'_{A-1}, n_{A-1}} (2n_{A-1} + 1) \\
&\quad - \delta_{n'_{A-1}+2, n_{A-1}} \sqrt{n_{A-1}^2 - n_{A-1}} - \delta_{n'_{A-1}-2, n_{A-1}} \sqrt{(n_{A-1}+1)(n_{A-1}+2)} \big) \bigg] \\
&\quad \times \langle N_{A-1} n_{A-1} \| N_A \rangle, \qquad (14)
\end{aligned}
$$

where we have suppressed the i_A's and i_{A-1}'s for simplicity after the first line. Intermediate summations over N_{A-1}, n_{A-1}, i_{A-1}, N'_{A-1}, n'_{A-1}, and i'_{A-1} are implicit.

In the same manner as the kinetic energy, we can recursively embed the potential in the A-particle space, starting with the two-body interaction between the first two particles. Because we are working in fully symmetrized few-body spaces we do not need to consider all pairwise interactions, but only one such pair and scale by the number of interactions. For instance, in the three-particle system the full two-body interaction is $V^{(2)} = V_{12} + V_{23} + V_{13} = 3V_{12}$. In a general A-particle space, this becomes $V^{(2)} = \binom{A}{2} V_{12}$. The matrix element of a two-body potential, V_{12}, in the relative coordinate harmonic oscillator basis, $|n_1\rangle$, is $\langle n'_1 | V_{12} | n_1 \rangle = \int \langle n'_1 | p'_1 \rangle \langle p' | V_{12} | p \rangle \langle p | n_1 \rangle \, dp \, dp'$ where the matrix elements of $\langle p' | V_{12} | p \rangle$ are given by Eq. (4).

Once in the oscillator basis, embedding in a larger particle space is a straightforward process. Starting with the two-body interaction, V_{12}, the two-body oscillator symmetric states are isolated using the projector $\langle N_2 i_2 | n_1 \rangle$ which picks out just the n_1-even states. Embedding this interaction in the three-particle space involves adding a new Jacobi coordinate, $|n_2\rangle$, to the existing system. With respect to the two-body interaction, V_{12}, this additional coordinate is associated with a delta function, δ_{n_2, n'_2}. Finally we obtain the symmetric three-particle states by using the projector, $\langle N_3 i_3 \| N_2 i_2; n_2 \rangle$. Multiplying by $\binom{3}{2} = 3$ gives us the full strength of the two-body interaction.

In general we can write this procedure as an expansion of the final A-particle symmetric space matrix elements of V_{12}:

$$
\begin{aligned}
\big(V_A^{(2)}\big)_{\rm sym} &= \langle N'_A i'_A | V_A^{(2)} | N_A i_A \rangle \equiv \binom{A}{2} \langle N'_A i'_A | V_{12} | N_A i_A \rangle \\
&= \langle N'_A \| N'_{A-1} n'_{A-1} \rangle \langle N'_{A-1} n'_{A-1} | V_A | N_{A-1} n_{A-1} \rangle \langle N_{A-1} n_{A-1} \| N_A \rangle \\
&= \langle N'_A \| N'_{A-1} n'_{A-1} \rangle \\
&\quad \times \langle N'_{A-1} n'_{A-1} | (V_{A-1})_{\rm sym} \delta_{n'_{A-1}, n_{A-1}} | N_{A-1} n_{A-1} \rangle \langle N_{A-1} n_{A-1} \| N_A \rangle \qquad (15)
\end{aligned}
$$

where again we have dropped the i_A's after the first line for simplicity and intermediate sums are implicit. We remind the reader that n_{A-1} can only take values from 0 to $N - N_{A-1}$, where N is the total oscillator quantum number used to organize the states. We start with the two-particle space and work our way up to the A-body space, embedding the interactions successively in each sector using Eq. (15). When symmetrizing V_A we must embed the symmetrized V_{A-1} with the appropriate combinatoric factor included as explained above. This factor derives from the fact that we had embedded a 2-body force in the $A-1$ space that is now to be extracted and embedded in the A-particle space. Thus we must remove the old factor $\binom{A-1}{2}$ and multiply by the new $\binom{A}{2}$ factor, which has the net effect of multiplying by $A/(A-2)$.

Any initial three-body force (discussed below) is embedded in the same manner as above except that it originates in the three-particle space. The initial three-body force is a function of two Jacobi momenta, which we transform directly into the partially symmetrized three-particle oscillator space and then use all of the same embedding procedures developed above. Note that two- and three-body forces must be embedded in higher spaces with different symmetry factors, $\binom{A}{2}$ and $\binom{A}{3}$, respectively.

In previous formulations of this recursive approach [9], subsequent potential embeddings are achieved by making a change of coordinates for the last two Jacobi momenta. For systems with $A > 5$, the three-body force requires a similar change of coordinates for the last three Jacobi momenta. Such a scheme is unnecessary here.

2.4. SRG evolution

As in Ref. [4], we apply the Similarity Renormalization Group (SRG) transformations to NN interactions based on the flow equation formalism of Wegner [2]. The evolution or flow of the Hamiltonian with a parameter s is a series of unitary transformations,

$$H_s = U_s H U_s^\dagger \equiv T_{\rm rel} + V_s, \tag{16}$$

where $T_{\rm rel}$ is the relative kinetic energy and $H = T_{\rm rel} + V$ is the initial Hamiltonian in the center-of-mass system. Eq. (16) defines the evolved potential V_s, since $T_{\rm rel}$ taken to be independent of s. Then H_s evolves according to

$$\frac{dH_s}{ds} = [\eta_s, H_s], \tag{17}$$

with

$$\eta_s = \frac{dU_s}{ds} U_s^\dagger = -\eta_s^\dagger. \tag{18}$$

Choosing η_s specifies the transformation, which is taken as the commutator of an operator, G_s, with the Hamiltonian,

$$\eta(s) = [G_s, H_s], \tag{19}$$

so that we obtain Eq. (1):

$$\frac{dH_s}{ds} = \big[[G_s, H_s], H_s\big]. \tag{20}$$

Applications to nuclear physics to date in a partial-wave momentum basis have primarily used $G_s = T_{\rm rel}$ [4] (see Ref. [7] for an alternative).

Once we have constructed a complete symmetrized basis for A particles (specified by the value of $N_{\max}$) and evaluated the Hamiltonian matrix elements in this basis, applying Eq. (20) with $G_s = T_{\rm rel}$ is immediate. That is, we have coupled, first-order differential equations for each matrix element of the Hamiltonian, with the right side of each equation given by a series of matrix multiplications. This is efficiently implemented in any computer language with matrix operations and differential equation solvers.

Individual matrix elements of the Hamiltonian obey the SRG's differential equations:

$$\begin{aligned}\frac{d}{ds}\langle N'_A i'_A|(V_A)_s|N_A i_A\rangle &= \langle N'_A i'_A|\big[[T, H_s], H_s\big]|N_A i_A\rangle \\ &= \langle N'_A i'_A|T H_s H_s|N_A i_A\rangle + \langle N'_A i'_A|H_s H_s T|N_A i_A\rangle \\ &\quad - 2\langle N'_A i'_A|H_s T H_s|N_A i_A\rangle. \end{aligned} \tag{21}$$

We have defined $dT/ds = 0$ so that all of the flow occurs in the matrix representation of the potential, $(V_A)_s$. Using the matrix representations of T and H_s in the $|N_A i_A\rangle$ basis, the right side of Eq. (21) is simply a series of matrix multiplications. The initial condition at $s = 0$ is the initial Hamiltonian, $\langle N'_A i'_A|T + V_A|N_A i_A\rangle$, which can have few-body components in V_A. We consider here both two-body-only and two-body plus a three-body component (for $A \geqslant 3$). In practice we often use the flow variable $\lambda = 1/s^{1/4}$; because there is no explicit s dependence in Eq. (1), switching variables is trivial.

To carry out the SRG evolution, we use a built-in MATLAB differential equation solver, such as the MATLAB function `ode23`, which is an implementation of a Runge–Kutta differential equation algorithm. We studied the running time to evolve the various SRG schemes (i.e., the choice of G_s) by plotting the time to run versus the evolution parameter, s. We find a straight line as s increases, indicating no stiffness, in every combination of potential and SRG scheme used to date.

The SRG induces few-body forces as it evolves an initial interaction in a few-particle space. To study the contributions of different few-body forces we must isolate these components of the full interaction. By definition the two-body force evolution keeps the $A = 2$ binding energy invariant under evolution. We can isolate the three-body force from the two-body matrix elements by embedding the evolved two-body-only force in the three-particle space and subtracting it from the full two-plus-three-body evolved interaction. In our MATLAB implementation these procedures take only a few lines of code.

3. Results

3.1. Initial ("Bare") interactions

The bulk of our calculations adopt a model from Ref. [13] that uses a sum of two Gaussians to simulate repulsive short-range and attractive mid-range nucleon–nucleon two-body potentials:

$$V^{(2)}(x) = \frac{V_1}{\sigma_1\sqrt{\pi}} e^{-x^2/\sigma_1^2} + \frac{V_2}{\sigma_2\sqrt{\pi}} e^{-x^2/\sigma_2^2} \tag{22}$$

or

$$V^{(2)}(p, p') = \frac{V_1}{2\pi\sqrt{2}} e^{-(p-p')^2\sigma_1^2/8} + \frac{V_2}{2\pi\sqrt{2}} e^{-(p-p')^2\sigma_2^2/8}, \tag{23}$$

Table 1
Parameter sets for the two-body potential of Eq. (23).

Name	V_1	σ_1	V_2	σ_2
V_α	12.0	0.2	−12.0	0.8
V_β	0.0	0.0	−2.0	0.8

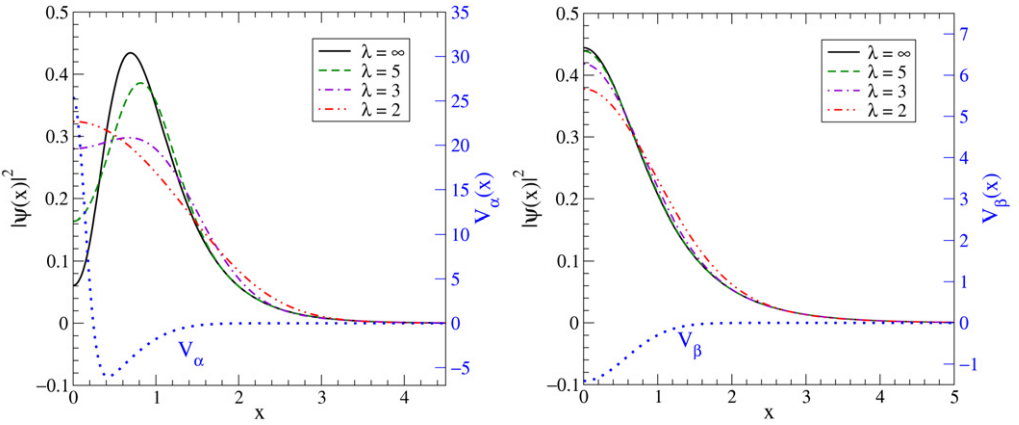

Fig. 1. (Color online.) Potentials (dotted line, with axis on right) and probability distributions (other lines, with axis on left) for the lowest two-body bound state as a function of $x = |x_1 - x_2|$ at different stages in the SRG evolution ($\lambda = 1/s^{1/4}$). The left plot is V_α and the right plot is V_β (see Table 1).

in units with $\hbar$ and the boson mass equal to one. The parameters used in Ref. [13] were chosen so that dimensionless ratios characterizing the one-dimensional saturation properties are qualitatively similar to the corresponding ratios of empirical three-dimensional properties. We also want to explore a range of parameters to test what behavior is general and what relies on specific features. We start with the parameters listed in Table 1; the potential V_α uses the parameters from Ref. [13] and is plotted in Fig. 1. We will fix the range of the attractive part and vary the relative strength and range of the repulsive parts and visa versa. We also vary the purely attractive potential V_β, which was used in Ref. [14] and is also plotted in Fig. 1. The eigenvalue problem for the relatively small matrices considered here can be solved by any conventional matrix diagonalization program (MATLAB was used here).

To test that the symmetrized harmonic oscillator basis was correctly constructed for $A = 2$, 3, and 4 (see below), we first diagonalized the Hamiltonian using the purely attractive Gaussian two-body potential V_β. The normalization is such that $V_\beta(x)$ becomes a delta function with strength V_2 as $\sigma_2 \to 0$ [14] (note the numerical factors from the Fourier transform because of our normalization of the Jacobi momenta). This limiting case has a known analytic solution for the (only) bound state of A bosons. For finite σ_2, we were able to confirm the accuracy of the diagonalizations as a function of the basis size $N_{\max}$ by comparison to coordinate-space stochastic variational method (SVM) calculations using a published code [15] adapted to one dimension [16].

We also explore the evolution of Hamiltonians with an initial three-body force. We choose a regulated contact interaction in the three-particle momentum space,

$$V^{(3)}(p, q, p', q') = c_E f_\Lambda(p, q) f_\Lambda(p', q'), \tag{24}$$

Table 2
Ground-state energies for two-body potentials from Table 1 with various strengths of the initial three-body potential Eqs. (24)–(25) with $\Lambda = 2$ and $n = 4$ for $A = 2$, 3, and 4.

$V^{(2)}$	c_E	E_2	E_3	E_4
V_α	−0.10	−0.920	−3.223	−7.125
V_α	−0.05	−0.920	−2.884	−5.832
V_α	−0.01	−0.920	−2.628	−4.906
V_α	0.00	−0.920	−2.567	−4.695
V_α	0.01	−0.920	−2.507	−4.494
V_α	0.05	−0.920	−2.278	−3.798
V_α	0.10	−0.920	−2.027	−3.179
V_β	−0.10	−0.474	−3.379	−8.412
V_β	−0.05	−0.474	−2.283	−5.727
V_β	−0.01	−0.474	−1.792	−4.183
V_β	0.00	−0.474	−1.708	−3.846
V_β	0.01	−0.474	−1.626	−3.517
V_β	0.05	−0.474	−1.370	−2.451
V_β	0.10	−0.474	−1.240	−1.874

where c_E is the strength of the interaction and the form factor f_Λ depends on the Jacobi momenta as

$$f_\Lambda(p,q) \equiv e^{-((p^2+q^2)/\Lambda^2)^n}. \tag{25}$$

The regulator cutoff Λ sets the scale of the fall-off in momentum and n determines the sharpness of this fall-off. This form is analogous to the regulated three-body contact interactions used in chiral effective field theory [17]. We have not explored in detail the impact of adjusting Λ and n but have focused on how the SRG handles a varying strength c_E. All results here are for $\Lambda = 2$ and $n = 4$.

Most of the figures in this paper show calculations with $N_{\max} = 28$. With this basis size, the ground-state energies are generally converged to one part in 10^4, which is more than sufficient for our purposes. We note that for a given oscillator parameter, $N_{\max}$ must be large enough so that both the short distance *and* long distance physics is adequately reproduced. As usual, increasing $N_{\max}$ leads to rapidly increasing matrix sizes and computation times; times for $A = 3$ with $N_{\max} = 32$ are a factor of 3 longer than with $N_{\max} = 28$ and with $N_{\max} = 40$ the time increases by another factor of 10. A sampling of ground-state energies are given in Table 2.

3.2. Two-body results

We first consider the bound state of two identical bosons using the potential V_α. Because the SRG is a series of unitary transformations, we expect that the binding energy will not be changed by evolving the two-body interaction in the two-particle space. Indeed, we find it to be constant to high accuracy. The ground-state wave function, however, changes dramatically, as seen from the probability densities plotted in Fig. 1. The initial probability density exhibits a sizable "wound" near the origin that is filled in as λ decreases. By $\lambda = 2$ there is no signature of a repulsive core (and the wave function is modified out to larger x). This is the same pattern seen for the S-wave component of deuteron wave functions starting from three-dimensional nucleon–nucleon S-wave potentials with strong repulsive cores such as Argonne v_{18}, with the "uncorrelated" final wave function at $\lambda = 2$ roughly comparable to $\lambda = 1.5$ fm^{-1} for the deuteron [5].

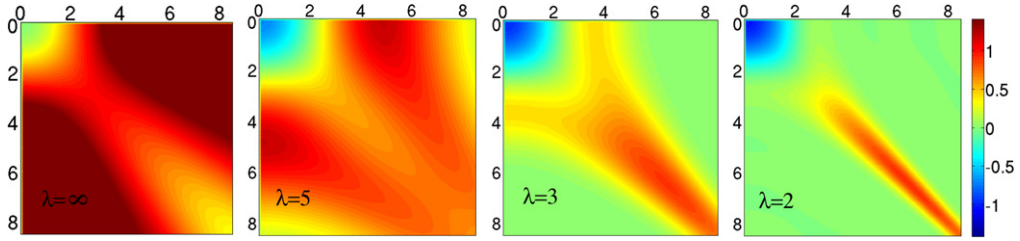

Fig. 2. (Color online.) Even part of the SRG potential $[V_s^{(2)}(p, p') + V_s^{(2)}(p, -p')]$ in dimensionless units as a function of p and p' for $\lambda = \infty$, 5, 3, and 2 (where $\lambda = 1/s^{1/4}$). The initial potential is V_α from Table 1.

The evolution of the potential in the momentum basis, shown as a color contour plot in Fig. 2, also demonstrates this behavior. (The even part of the potential is shown, which is the analog of the S-wave part.) The initial potential is dominated by strongly repulsive matrix elements coupling low and high momenta. The evolution in λ band diagonalizes the potential to a width in p^2 of roughly λ^2 while a soft attractive part emerges in the low-momentum region. The pattern in Fig. 2 reflects increasing non-locality as λ is lowered, which in turn reduces the wound in the wave function. From the probability density and the momentum space plots we estimate that evolving to halfway between $\lambda = 2$ and 3 for V_α corresponds roughly to the λ scale typically used in nuclear structure calculations (around 2 fm^{-1}).

3.3. Three-body results

To calculate properties of the three-particle system we construct the Hamiltonian in the basis of symmetric three-particle eigenstates as described in Section 2.3. The SRG evolution of the potential in the three-particle space leaves the ground state energy invariant if the full Hamiltonian is kept, because the transformations are unitary. However, the Hamiltonian matrix elements in this space do not follow simply from the pairwise sum of the two-body potential matrix elements; as the SRG evolves a three-body force is induced even if its initial strength is zero.

The effect of this full three-particle space SRG evolution is shown in Fig. 3 for initial two-body potential V_α and with initial $V^{(3)} = 0$ (non-zero values of c_E are considered in the next section). We plot the ground-state energy for the three-particle system both with the initial two-body interaction embedded in the three-particle symmetric space and then evolved (the red curve with squares) and also with the two-body interaction evolved in the two-particle space before embedding in the three-particle space at each λ (the black curve with circles). We can see that the energy evaluated with the two-body interaction alone deviates noticeably as λ drops below 10. This variation is the signature that the two-body transformation is only approximately unitary in the three-particle sector. The error reaches a peak in λ between 2 and 3 and then decreases. The same pattern has been observed for NN potentials in three dimensions [6] and remains qualitatively the same when parameters in the potential are varied (e.g., see the right plot in Fig. 3). We made the same calculation using the purely attractive initial two-body potential V_β, which is shown in Fig. 4. Here the induced three-body force has the opposite sign and there is no maximum, which implies that the qualitative pattern of evolution is dictated by the interplay between attractive long-range and repulsive short-range parts of the potential. These features are explored further in Section 3.5.

In Fig. 5 we test SRG decoupling [12] within the harmonic oscillator basis. The left panel shows the results when only the two-body evolved potential is used to calculate $A = 3$ binding

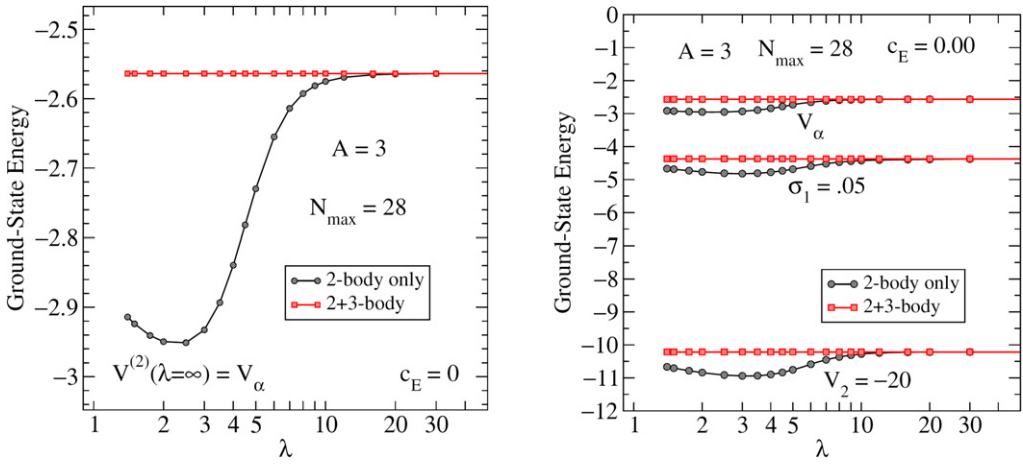

Fig. 3. (Color online.) The lowest bound-state energy E_3 for a three-particle system as a function of λ with the initial two-body-only potential V_α. The (red) curves with squares include the full evolution of the Hamiltonian while the (black) curves with circles use the two-body potential evolved in the two-particle system. The right frame shows two additional results from varying σ_1 and V_2 from the values in Table 1.

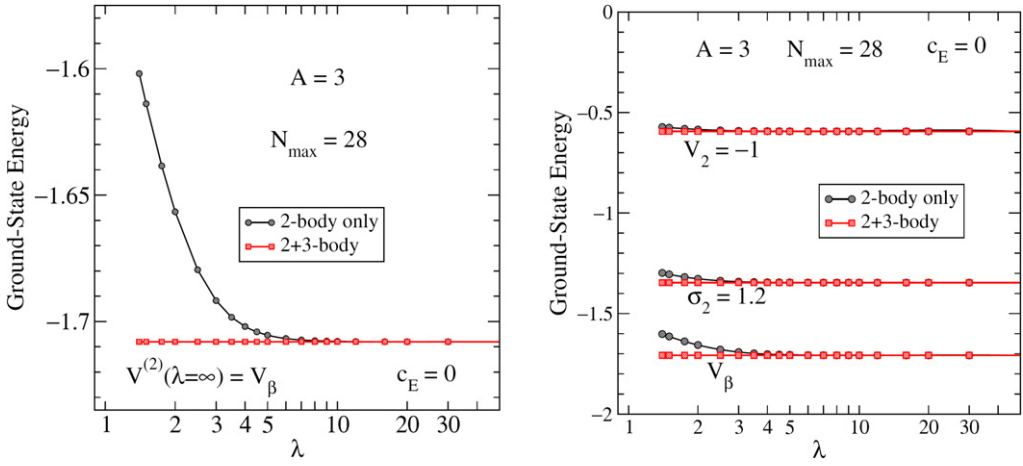

Fig. 4. (Color online.) Same as Fig. 3 but with initial potential V_β. The right frame shows two additional results from varying σ_2 and V_2 from the values in Table 1.

energies. In the right panel, the potential was evolved in the full three-body space, allowing three-body forces to be induced. The Hamiltonians for selected λ values are diagonalized in bases of decreasing size, as measured by "N_{cut}", which is the cut-off applied to the potential to study its decoupling properties. (That is, the potential is set to zero for matrix elements for which one or both states has $N > N_{\text{cut}}$.) The degree of decoupling is measured by the point of departure, as N_{cut} is lowered, from the asymptotic energy for $N_{\max} = 40$. As the potential is evolved from the initial potential ($\lambda = \infty$) down to $\lambda = 2.5$, decoupling is achieved for smaller spaces, which means convergence is reached for smaller basis sizes. This is the same pattern as found for realistic NN potentials [12].

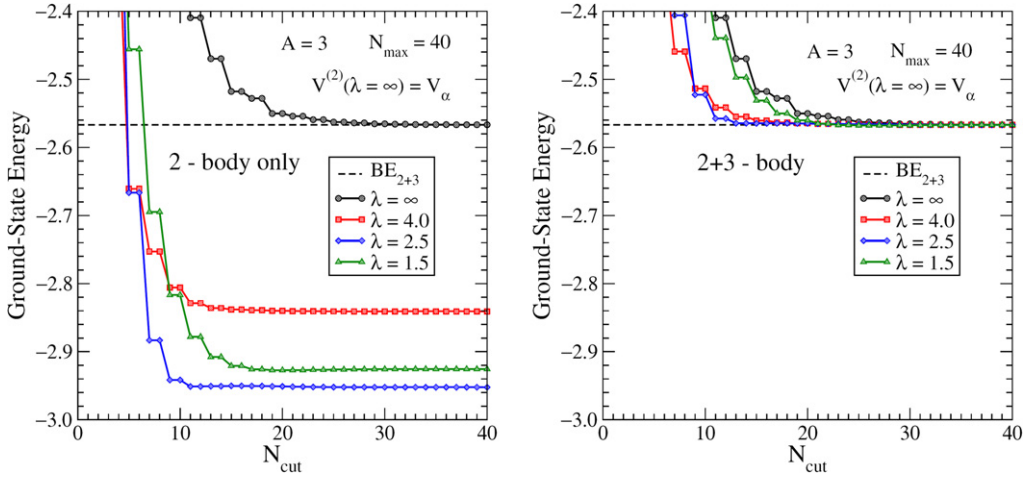

Fig. 5. (Color online.) Decoupling in the three-particle system. The initial V_α potential is evolved to each λ shown in a basis with $N_{\max} = 40$. On the left only the two-body potential is kept while the full potential is kept on the right. Matrix elements of the potential are set to zero if one or both states have $N > N_{\text{cut}}$ and the resulting Hamiltonian is diagonalized to obtain the ground-state energies plotted.

In the left panel of Fig. 5, the ground-state energies asymptote to different values because the evolution is not completely unitary. One might imagine that this would affect the decoupling, but we show this is not the case here. In the right panel, the induced three-body interaction is kept, so the curves asymptote to the same energy at large $N_{\max}$, while the same pattern of decoupling is observed. We note that the decoupling benefits afforded by evolution in the oscillator basis are less straightforward than in the two-body momentum basis studied for NN in [12]. In particular the cut-off errors *increase* for λ smaller than the point at which the two-body-only binding energy is at a minimum (i.e., for $\lambda = 1.5$ in Fig. 5).

3.4. Results for $A = 4$ and $A = 5$

Next we turn to $A = 4$ and $A = 5$, where we expect to see the effects of induced three-, four- and five-body forces. The key issue is the relative sizes of these contributions; we are looking to test whether an initial hierarchy of few-body interactions is preserved and therefore can be truncated with a controlled error. (Of course, generalizing these results to three dimensions will require repeating these tests for real 3D nuclei.)

In applying the SRG in the four-particle space we have three different calculations of the ground-state energy to compare. The first is the two-body potential embedded successively in the three- and four-particle spaces and then evolved in the four-particle space. The resulting unitary transformations will induce three- and four-body interactions that leave the eigenvalues invariant. We can also evolve in the two-particle space before embedding in the three- and four-particle spaces and diagonalizing. As we saw before in Fig. 3 and see now in Fig. 6, the two-body-only evolution deviates because the Hamiltonian is not evolved by an exactly unitary transformation. Finally, to find the relative size of the three and four-body interactions we can evolve in the three-particle space, thereby inducing only three-body forces. Note that the two and three-body forces must be embedded differently in the four particle space because they have different combinatoric factors associated with them, i.e., there are $\binom{4}{2} = 6$ pairs and $\binom{4}{3} = 4$ triplets. So, the proper

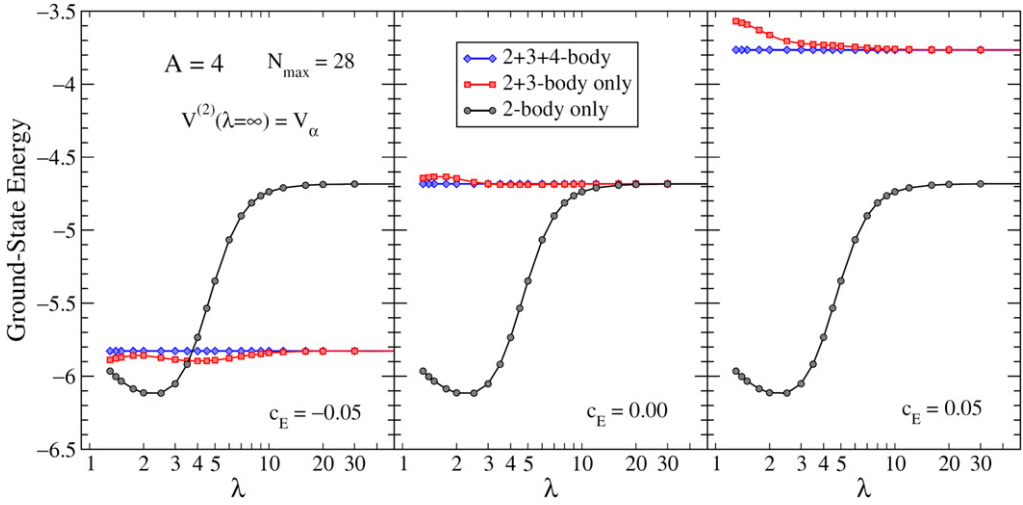

Fig. 6. (Color online.) The lowest bound-state energy E_4 for a four-particle system as a function of λ with the initial two-body potential V_α and different initial three-body force strengths ($c_E = \pm 0.05$).

mixture of two- and three-body force contributions to the four-particle system interaction is $V = 6V^{(2)} + 4V^{(3)}$.

All three of these calculations for $A = 4$ are shown in Fig. 6 for the two-body potential V_α and several choices of the initial three-body force. The magnitude of c_E was chosen so that the fractions of the $A = 3$ and $A = 4$ ground-state energies from the three-body interaction are roughly comparable to the corresponding fractions for nuclei using typical realistic NN potentials. The qualitative behavior is similar for other choices of c_E and $V^{(2)}$. In all plots the curves for the two-body-only (black line with circles), the two-plus-three (red line with squares), and the full two-plus-three-plus-four interaction (blue line with diamonds) show the hierarchy of different few-body interaction components. The difference between the square and diamond lines represents the contribution of the four-body force, and the difference between the circle and square lines is the contribution of the three-body force alone. In the left and right panels, the latter contribution is the sum of initial and induced three-body forces.

The four-body contribution is at most ten percent that of the three-body, which is itself small compared to the two-body contribution except when the latter gets small for small λ (note the expanded scales on the figures). Considering calculations with different c_E values, we see that the λ dependence of the induced four-body part depends on the interplay of initial and induced forces. In some cases noticeable (but small) evolution starts at $\lambda = 10$ while in other cases it is deferred until much smaller λ. Regardless of the details, we stress that there is no sign that induced many-body forces have rapid growth with A or exhibit unusual scaling.

We repeated for $A = 4$ our test of decoupling that was shown in Fig. 5 for $A = 3$. A similar pattern of decoupling is found, namely an increased degree of decoupling until a λ corresponding to the minimum of the two-body-only ground-state energy of the $A = 4$ system, after which it deteriorates.

In Fig. 7 we show results for the SRG evolution, with initial potential V_α and no initial three-body interactions, in a five-particle system for several values of $N_{\max}$. The right panel, with $N_{\max} = 28$, shows the converged result. We see a decreasing hierarchy of induced many-body contributions for all λ; the five-body contribution is essentially negligible (or not distinguishable

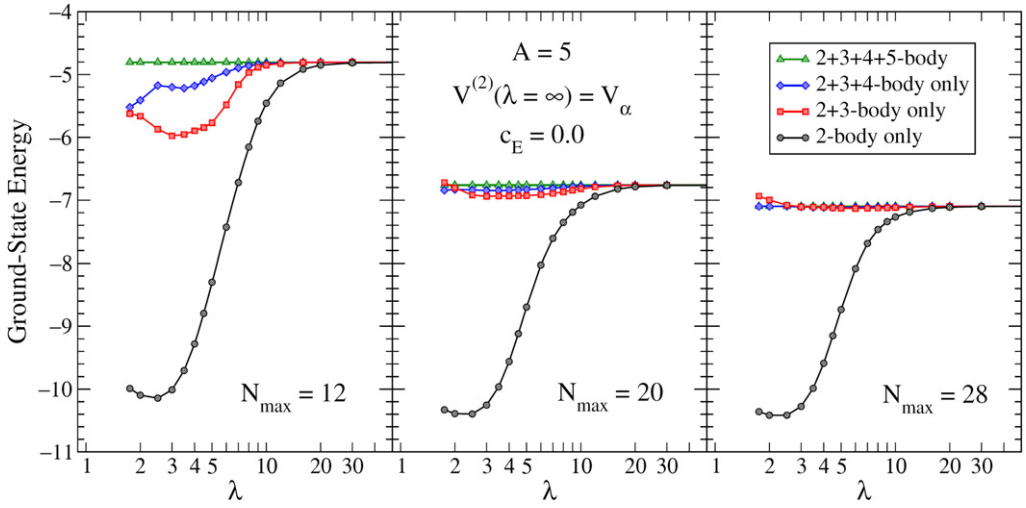

Fig. 7. (Color online.) The lowest bound-state energy E_5 for a 5-particle system as a function of λ with an initial two-body-only V_α potential for several values of $N_{\max}$.

from numerical noise). Differences at the lower $N_{\max}$ sized spaces arise both because the space needs to be large enough for convergence to the exact energy eigenvalues but also because the initial evolution of the potential needs a sufficiently large space. Decoupling may improve this feature but is dependent on the type of SRG used and the basis in which it is implemented. This is important to keep in mind for the generalization to the realistic nuclear problem.

3.5. Analysis of three-body force running

In this section we examine how induced three-body interactions evolve in our one-dimensional laboratory and make connections to the diagrammatic expansion developed in Ref. [8]. As raw material for this analysis, we plot in Fig. 8 the error of the evolving two-body-only binding energy while varying several parameters of the initial two-body interaction V_α for $A = 3$ ground-state energies. In the left plots we vary the range (top) and the strength (bottom) of the attractive part of V_α. In the right plots we vary the range (top) and the strength (bottom) of the repulsive part. In Fig. 9 we present similar plots for a simpler system that starts with the initial attraction-only two-body potential V_β.

Certain qualitative features are found as expected in these figures. Shorter ranges imply enhanced coupling from low to high momentum and therefore we anticipate that the evolution will start sooner (i.e., at higher λ). This is seen clearly on the left in Fig. 9 and for the variation of the (shorter-ranged) repulsive potential in Fig. 8 (top right plot). There is also an unsurprising increase in the magnitude of the induced three-body interaction at each λ with increased magnitude of the potential, as seen on the right in Fig. 9 and on the bottom left in Fig. 8. For a more definitive analysis we need to recall the discussion from Ref. [8].

The SRG evolution equation for the three-particle sector in the notation of Ref. [8] is

$$\frac{dV_s^{(2)}}{ds} + \frac{dV_s^{(3)}}{ds} = \overline{\overline{V}}_s^{(2)} + \overline{\overline{V}}_s^{(3)} + \left[\overline{V}_s^{(2)}, V_s^{(2)}\right] + \left[\overline{V}_s^{(2)}, V_s^{(3)}\right] + \left[\overline{V}_s^{(3)}, V_s^{(2)}\right] + \left[\overline{V}_s^{(3)}, V_s^{(3)}\right], \tag{26}$$

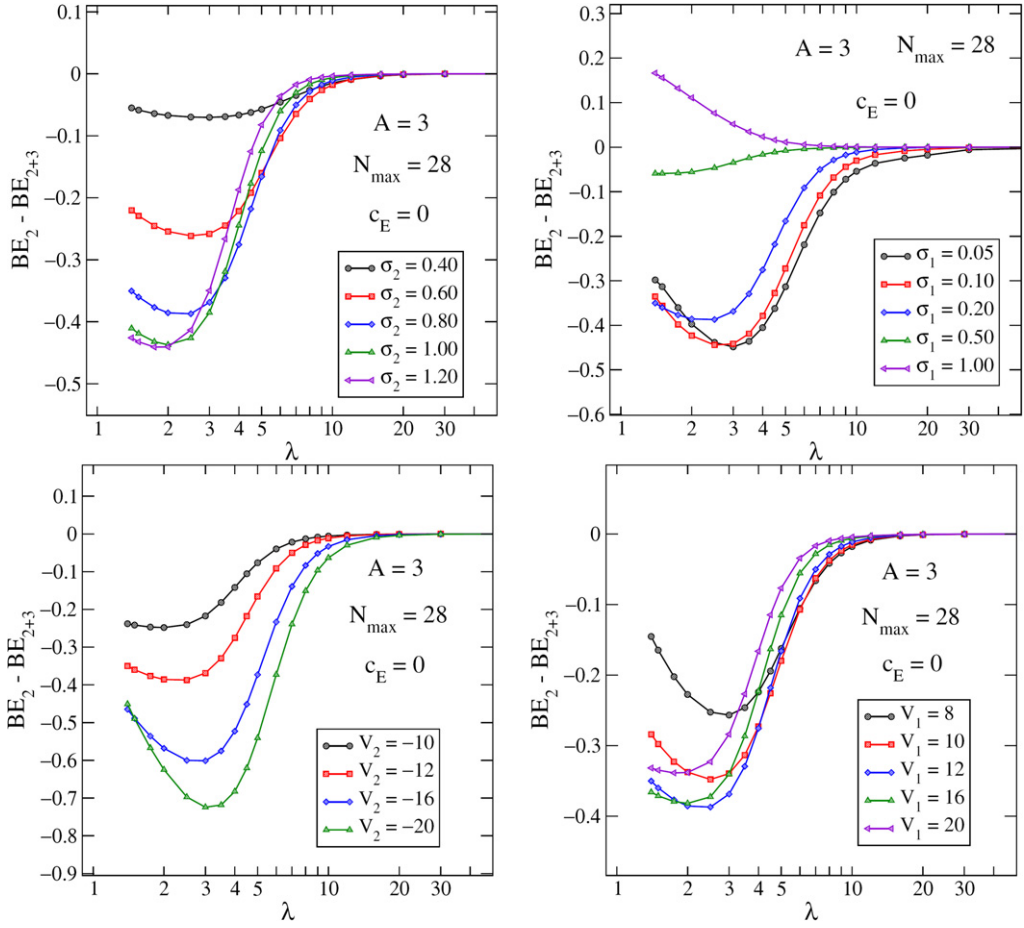

Fig. 8. (Color online.) Differences of two-body-only and two-plus-three-body $A = 3$ ground-state energies as a function of λ. Each of the parameters of the potential V_α are varied in each plot as the other parameters are held constant. The upper panels vary the ranges while the lower vary the strengths; the left vary the attractive part and the right vary the repulsive part.

where each bar denotes a commutator with $T_{\rm rel}$. We remind the reader that $dT_{\rm rel}/ds = 0$ by construction. A diagrammatic decomposition of this equation is shown in Fig. 10. In the two-body sector, the equation reduces to the first term on the left and the first and third terms on the right (the first row in Fig. 10). These terms keep two-particle energy eigenvalues invariant under evolution. In the three-particle sector, Eq. (26) results in not only these two-body graphs with a disconnected spectator but additional graphs involving connected combinations of two and three-body interactions. The diagrams with two-body interactions and a disconnected spectator line satisfy the two-body evolution equations, and so will cancel out of the full three-particle-sector evolution equation. Thus the evolution of the three-body interaction is dictated by the connected diagrams (the second row in Fig. 10). In summary, the evolution of the A-body potential in the A-particle system is given by

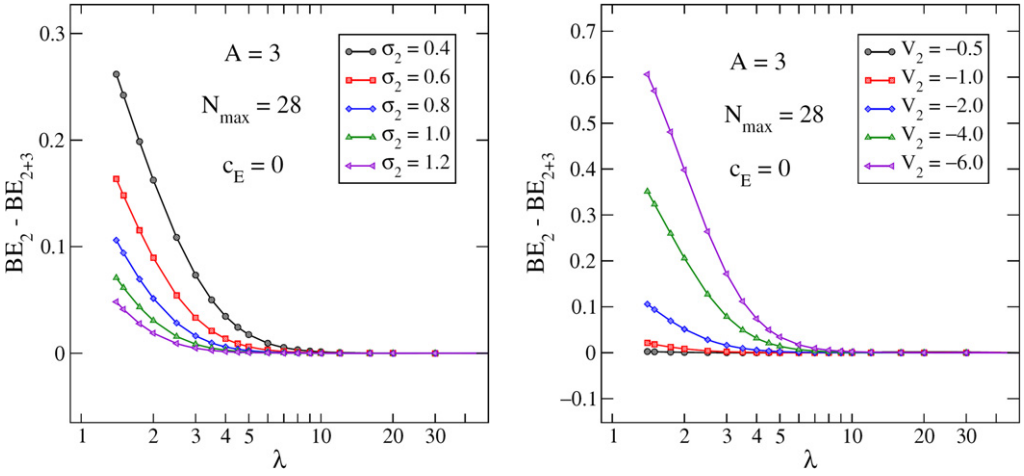

Fig. 9. (Color online.) Same as Fig. 8 but for V_β.

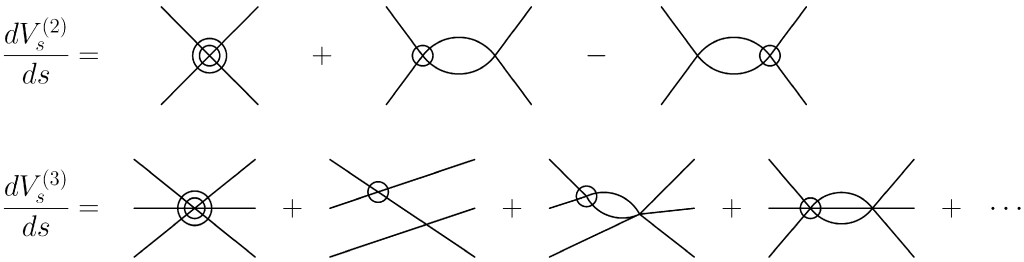

Fig. 10. A diagrammatic decomposition of the SRG equation (26). A circle at a vertex denotes a commutator with T_{rel}.

$$\frac{dV_s^{(A)}}{ds} = [\eta_s, H_s]_A, \tag{27}$$

where the "A" subscript on the right side means the fully connected A-particle terms.

To make a connection between the individual terms in the three-body interaction evolution and the running of the ground-state energy, we need to derive the evolution equations for the *expectation value* of $V_s^{(3)}$ in the ground state. Denoting the ground-state wave function for the A-particle system by $|\psi_s^A\rangle$, it evolves according to

$$|\psi_s^A\rangle = U_s|\psi_{s=0}^A\rangle, \qquad \frac{d}{ds}|\psi_s^A\rangle = \eta_s|\psi_s^A\rangle, \tag{28}$$

where U_s is the SRG unitary transformation at s and

$$\eta_s = \frac{dU_s}{ds}U_s^\dagger = -\eta_s^\dagger. \tag{29}$$

Then the matrix element of an operator O_s evolves according to

$$\frac{d}{ds}\langle\psi_s^A|O_s|\psi_s^A\rangle = \langle\psi_s^A|\frac{dO_s}{ds} - [\eta_s, O_s]|\psi_s^A\rangle. \tag{30}$$

If the operator O_s evolves according to $O_s = U_s O_{s=0} U_s^\dagger$, then the matrix element vanishes, as when $O_s = H_s$.

However, if we wish to see how one part of H_s evolves, such as the expectation value of $V^{(3)}$, we obtain

$$\frac{d}{ds}\langle\psi_s^A|V_s^{(3)}|\psi_s^A\rangle = \langle\psi_s^A|\frac{dV_s^{(3)}}{ds} - \big[\eta_s, V_s^{(3)}\big]|\psi_s^A\rangle, \tag{31}$$

which does not give zero in general because $V_s^{(3)} \neq U_s V_{s=0}^{(3)} U_s^\dagger$. In the two-particle case, the analog of Eq. (31) gives $d\langle V^{(2)}\rangle/ds = \langle[\eta_s, T_{\rm rel}]\rangle$. In the three-particle case, we can expand Eq. (31) as

$$\begin{aligned}
\frac{d}{ds}\langle\psi_s|V_s^{(3)}|\psi_s\rangle &= \langle\psi_s|[\eta_s, H_s]_3 - \big[\eta_s, V_s^{(3)}\big]|\psi_s\rangle \\
&= \langle\psi_s|\big[\overline{V}_s^{(3)}, T_{\rm rel}\big] + \big[\overline{V}_s^{(2)}, V_s^{(2)}\big]_c + \big[\overline{V}_s^{(2)}, V_s^{(3)}\big] + \big[\overline{V}_s^{(3)}, V_s^{(2)}\big] \\
&\quad + \big[\overline{V}_s^{(3)}, V_s^{(3)}\big] - \big[\overline{V}_s^{(2)}, V_s^{(3)}\big] - \big[\overline{V}_s^{(3)}, V_s^{(3)}\big]|\psi_s\rangle \\
&= \langle\psi_s|\big[\overline{V}_s^{(3)}, H_s\big] + \big[\overline{V}_s^{(2)}, V_s^{(2)}\big]_c - \big[\overline{V}_s^{(3)}, V_s^{(3)}\big]|\psi_s\rangle \\
&= \langle\psi_s|\big[\overline{V}_s^{(2)}, V_s^{(2)}\big]_c - \big[\overline{V}_s^{(3)}, V_s^{(3)}\big]|\psi_s\rangle,
\end{aligned} \tag{32}$$

where $\overline{V}_s^{(2)}$ and $\overline{V}_s^{(3)}$ are the commutators $\overline{V}_s^{(2)} = [T_{\rm rel}, V_s^{(2)}]$ and $\overline{V}_s^{(3)} = [T_{\rm rel}, V_s^{(3)}]$. In the third line, the expectation value of the commutator, $[\overline{V}_s^{(3)}, H_s]$, vanishes identically.

The term with the subscript "c" has had the two-body disconnected diagrams removed. In our MATLAB implementation, this subtraction is achieved by first embedding the two-particle-space evolved version of this commutator in the three-particle space. Computing $[\overline{V}_s^{(2)}, V^{(2)}]$ in the two-particle space alone involves only the one-loop two-body interactions, so embedding in the three-particle sector results in only the disconnected parts. This disconnected part can then be subtracted from the total three-particle sector version of the same commutator, leaving only the three-particle fully connected part.

It is most useful for our analysis to convert from derivatives with respect to s to derivatives with respect to λ using $\frac{d}{ds} = -\frac{\lambda^5}{4}\frac{d}{d\lambda}$. In Fig. 11 we show the ground-state expectation values of the right side of Eq. (31), which are broken down into the two terms from the right side of Eq. (32) for $A = 3$ and various potentials. It is apparent that the drivers of three-body matrix element evolution depend on the interplay between long- and short-range, attractive and repulsive parts. The lower right panel of Fig. 11 shows an increasing attractive strength of the three-body force when starting from an attractive-only two-body potential. In this regime the dominant contribution to the evolution of the three-body potential matrix element is the tree-level two-body connected part $[\overline{V}_s^{(2)}, V_s^{(2)}]_c$. This observation accounts for the behavior in the right graph of Fig. 9, where the size of the error scales (roughly) like $(V^{(2)})^2$. Varying the long-range attraction strength in Fig. 8 shows a similar effect.

More generally, the impact on ground-state energies of the induced three-body interaction depends on the details of the correlations in the wave function. The other plots in Fig. 11 for the more realistic initial two-body potential, V_α, show the interplay between two- and three-body contributions to the three-body matrix element evolution. The three-body contribution to the three-body evolution stays small until the longer-range attractive part of the potential begins to affect the evolution. Most of the change is from $\lambda = 8$ to $\lambda = 3$, which is dominated by $\langle\overline{V}^{(2)}, V^{(2)}\rangle$. Thus, the feedback of the three-body potential depends on the initial conditions, but in general insures that the binding energy contribution stays small.

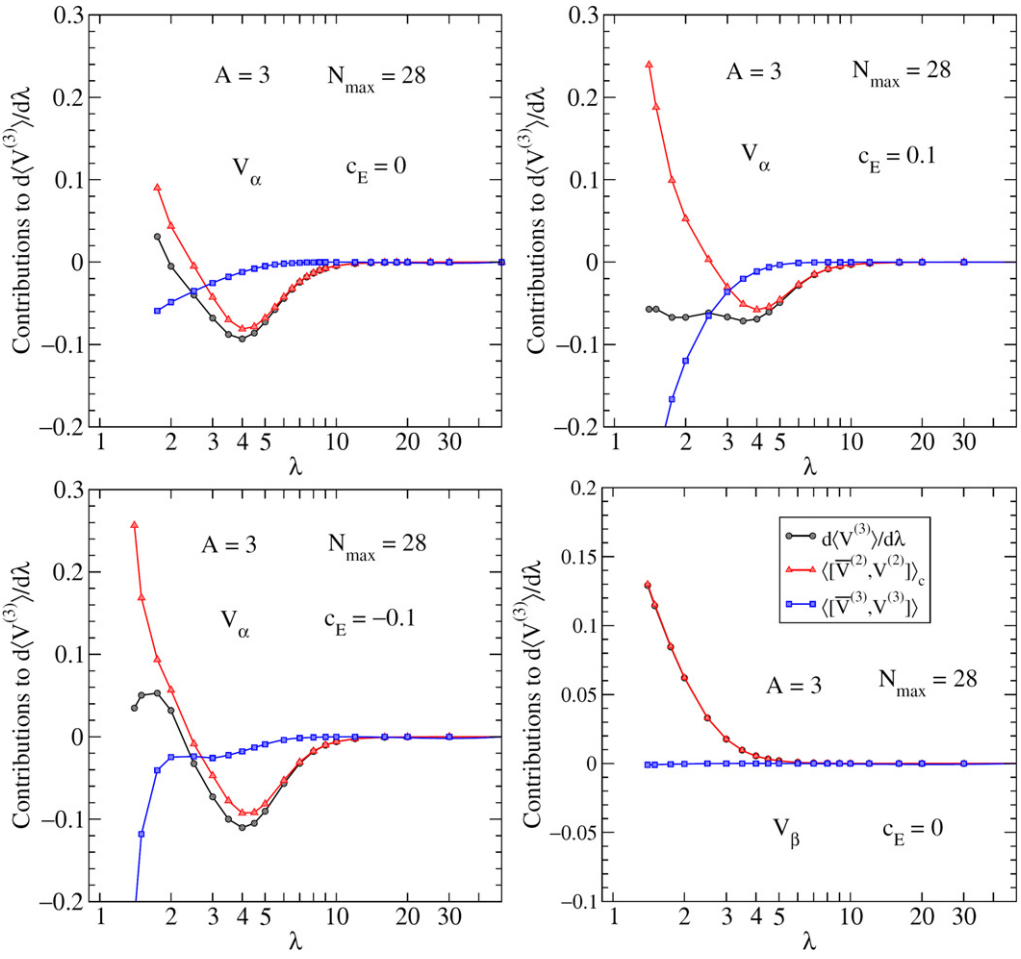

Fig. 11. (Color online.) Contributions from individual terms to the $A = 3$ ground-state expectation value $d\langle V_\lambda^{(3)}\rangle/d\lambda$ for several different two- and three-body potentials, as indicated in the plots. We emphasize that $\lambda \leqslant 2$ is very small, comparable to $\lambda \leqslant 1.5$ fm^{-1} for NN forces in analogous calculations with the NCSM [6].

We can repeat the above analysis for $A \geqslant 4$ and find no fully connected terms with only two-body forces. Again, disconnected terms involving two and three body potentials cancel out in the lower sectors. The leading terms are commutators with one $V_s^{(2)}$ and one $V_s^{(3)}$, followed by connected terms quadratic in $V_s^{(3)}$ and one term quadratic in $V_s^{(4)}$. All terms are small and additional cancellations among them further suppress the four-body contribution. Thus, the initial hierarchy of many-body forces implies that induced four-body (and higher-body) forces will be small.

4. Summary

In this paper we use a one-dimensional system of bosons with short-range repulsion and mid-range attraction as a laboratory to explore the evolution of many-body forces with the SRG. These

calculations serve as a proof-of-principle that induced few-body interactions can be calculated without solving T-matrix equations, as necessary in other renormalization group approaches. They establish that working within a harmonic oscillator basis is practical, although the generalization to three dimensions will be much more computationally intensive. This generalization is direct, however, because the recursive construction of properly symmetrized few-body basis states used here has already been carried out in the context of no-core shell model calculations [9–11]. The first steps with an $A = 3$ nuclear system will be taken soon, with the resulting three-body matrix elements then used as input to calculations in larger nuclei.

The patterns of SRG evolution observed in our one-dimensional laboratory have many similarities to those observed in three dimensions with realistic nuclear interactions. This includes, for example, decoupling in few-body systems, which was studied for nuclei with two-body forces only [12]. Here we find decoupling is unchanged when induced three-body interactions are included. Results for the contributions of induced three-body forces to ground-state energies show the same pattern of running observed for nuclear forces when a model two-body potential with short-range repulsion and long-range attraction is used. Differences in the running when an attractive-only two-body potential is used are understood in terms of the dominant contribution to the evolution equation for the three-body potential. Starting from an initial decreasing hierarchy of forces (two-body larger than three-body and all higher-body forces zero), the hierarchy is maintained for useful ranges of the SRG evolution. Induced four- and five-body forces are found to be very small. This is encouraging for the applications to realistic nuclei, but of course is not conclusive.

In a future study, we will use the one-dimensional laboratory to test alternative methods to evolve many-body interactions. These include the use of a Slater determinant basis of harmonic oscillators ("m scheme") and evolution in momentum space applying the diagrammatic methods from Ref. [8], which will allow us to cleanly assess the impact of the oscillator basis on the long-range physics both for the initial interaction and the SRG evolution. With the oscillator basis methods we will also consider evolving with a choice of the SRG generator G_s that is diagonal in the basis (i.e., $G_s = H_{\rm osc}$). The block diagonalization characteristic of "$V_{\rm low\,k}$" potentials (as opposed to band diagonalization as studied here) has been demonstrated for $A = 2$ in the SRG using a different choice for the flow operator G_s. We will explore whether this can be extended to $A \geqslant 3$, which would circumvent the need to solve coupled T-matrix problems. We will also test two alternatives to explicitly evolved few-body forces. One alternative is to evolve the two-body interaction only and fit an EFT-motivated few-body interaction at each λ, as currently done for nuclear applications of the SRG. Preliminary calculations find that 90% or more of the three-body contribution to the energy for $A > 3$ is captured by a single short-range three-body force with fixed cutoff Λ; further studies will test whether the Λ dependence is reduced appropriately when a gradient term is also fit. A second alternative is to use a normal-ordering prescription in the SRG to generate "density-dependent" two-body interactions. Finally, another avenue to explore is the evolution of other operators in few-body systems.

Acknowledgements

This work was supported in part by the National Science Foundation under Grant No. PHY-0653312 and the UNEDF SciDAC Collaboration under DOE Grant DE-FC02-07ER41457. We thank E. Anderson, S. Bogner, R. Perry, L. Platter, J. Drut, and A. Schwenk for their comments and discussions.

Appendix A. Transformation brackets

Transformation brackets are the expansion coefficients in the oscillator basis of one system of coordinates in terms of another [18,19]. We apply them to relate two different choices of Jacobi coordinates. Here we show the relevant transformation using the three-particle harmonic oscillator states defined in Eq. (5) and then generalize at the end.

The single particle momenta are k_1, k_2, and k_3. The unprimed Jacobi momenta [see Eq. (3)] are

$$\begin{aligned} p_1 &= \frac{1}{\sqrt{2}}(k_1 - k_2), \\ p_2 &= \sqrt{\frac{2}{3}}\big((k_1 + k_2)/2 - k_3\big), \end{aligned} \tag{A.1}$$

and the primed coordinates are obtained from exchanging k_2 and k_3:

$$\begin{aligned} p'_1 &= \frac{1}{\sqrt{2}}(k_1 - k_3), \\ p'_2 &= \sqrt{\frac{2}{3}}\big((k_1 + k_3)/2 - k_2\big). \end{aligned} \tag{A.2}$$

After some algebra, the transformation that exchanges the last two particles (i.e., k_2 and k_3) can be written as

$$\begin{pmatrix} p'_1 \\ p'_2 \end{pmatrix} = \begin{pmatrix} \frac{1}{2} & \frac{\sqrt{3}}{2} \\ \frac{\sqrt{3}}{2} & -\frac{1}{2} \end{pmatrix} \begin{pmatrix} p_1 \\ p_2 \end{pmatrix} \tag{A.3}$$

which enables us to express the primed oscillator states in terms of the unprimed ones.

We denote the three-particle oscillator basis by $|n_1 n_2\rangle = \eta_1^\dagger \eta_2^\dagger |0\rangle$ where we have set $\hbar\omega = 1$ for simplicity in this appendix (note that the transformation brackets will not depend on the value of $\hbar\omega$). The transformation that exchanges the last two single-particle coordinates can again be written as

$$\begin{pmatrix} \eta'_1 \\ \eta'_2 \end{pmatrix} = \begin{pmatrix} \frac{1}{2} & \frac{\sqrt{3}}{2} \\ \frac{\sqrt{3}}{2} & -\frac{1}{2} \end{pmatrix} \begin{pmatrix} \eta_1 \\ \eta_2 \end{pmatrix}. \tag{A.4}$$

The derivation of the harmonic oscillator transformation bracket follows directly as

$$\begin{aligned} \langle n'_1 n'_2 | n_1 n_2 \rangle_3 &= \langle 0 | \frac{1}{\sqrt{n_1! n_2! n'_1! n'_2!}} \eta_1'^{n'_1} \eta_2'^{n'_2} \eta_1^{\dagger n_1} \eta_2^{\dagger n_2} |0\rangle \\ &= \langle 0 | \frac{1}{\sqrt{n_1! n_2! n'_1! n'_2!}} \left[\frac{\eta_1}{2} + \frac{\sqrt{3}\eta_2}{2}\right]^{n'_1} \left[\frac{\sqrt{3}}{2}\eta_1 - \frac{1}{2}\eta_2\right]^{n'_2} \eta_1^{\dagger n_1} \eta_2^{\dagger n_2} |0\rangle \\ &= \langle 0 | \frac{1}{\sqrt{n_1! n_2! n'_1! n'_2!}} \sum_{k=0}^{n'_1} \binom{n'_1}{k} \left[\frac{1}{2}\eta_1\right]^{n'_1 - k} \left[\frac{\sqrt{3}}{2}\eta_2\right]^k \\ &\quad \times \sum_{j=0}^{n'_2} \binom{n'_2}{j} \left[\frac{\sqrt{3}}{2}\eta_1\right]^{n'_2 - j} \left[-\frac{1}{2}\eta_2\right]^j \eta_1^{\dagger n_1} \eta_2^{\dagger n_2} |0\rangle \end{aligned}$$

$$
\begin{aligned}
&= \frac{1}{\sqrt{n_1!n_2!n_1'!n_2'!}} \sum_{k=0}^{n_1'} \sum_{j=0}^{n_2'} \binom{n_1'}{k} \binom{n_2'}{j} \left[\frac{1}{2}\right]^{n_1'-k+j} \left[\frac{\sqrt{3}}{2}\right]^{n_2'-j+k} (-1)^j \\
&\quad \times n_1!n_2!\delta_{n_1'-k+n_2'-j,n_1}\delta_{k+j,n_2} \\
&= \sqrt{\frac{n_1!n_2!}{n_1'!n_2'!}} \sum_{k=0}^{n_1} \binom{n_1'}{k} \binom{n_2'}{n_2-k} \left[\frac{1}{2}\right]^{n_1'+n_2-2k} \left[\frac{\sqrt{3}}{2}\right]^{n_2'-n_2+2k} (-1)^{n_2-k}.
\end{aligned}
\tag{A.5}
$$

The second line is obtained from operating the transformation on the creation operators $\eta_s^\dagger$. The third line is the application of the binomial theorem. The fourth balances the oscillator creation and annihilations, and the fifth is just some simplification.

In the general A-particle system the transformation to exchange the last two particles, k_{A-1} and k_A, can be written as

$$
\begin{pmatrix} \eta'_{A-2} \\ \eta'_{A-1} \end{pmatrix} = \begin{pmatrix} \sqrt{\frac{1}{d+1}} & \sqrt{\frac{d}{d+1}} \\ \sqrt{\frac{d}{d+1}} & -\sqrt{\frac{1}{d+1}} \end{pmatrix} \begin{pmatrix} \eta_{A-2} \\ \eta_{A-1} \end{pmatrix}, \tag{A.6}
$$

where $d = (A-1)^2 - 1$ is the number of generators of the rotation group, $U(A-1)$, or the group $U(A)$ with the center of mass coordinate held fixed. An expression for the bracket $\langle n_{A-2}n_{A-1}|n'_{A-2}n'_{A-1}\rangle_{A(A-2)}$, which appears in Eq. (9), is obtained from Eq. (A.5) by substituting the general coordinate transformation Eq. (A.6) for the three-particle transformation Eq. (A.4), or $\sqrt{1/(d+1)}$ and $\sqrt{d/(1+d)}$ for $1/2$ and $\sqrt{3}/2$.

References

[1] S.D. Glazek, K.G. Wilson, Phys. Rev. D 48 (1993) 5863;
S.D. Glazek, K.G. Wilson, Phys. Rev. D 49 (1994) 4214.
[2] F. Wegner, Ann. Phys. (Leipzig) 3 (1994) 77.
[3] J. Kehrein, The Flow Equation Approach to Many-Particle Systems, Springer, Berlin, 2006.
[4] S.K. Bogner, R.J. Furnstahl, R.J. Perry, Phys. Rev. C 75 (2007) 061001.
[5] S.K. Bogner, R.J. Furnstahl, R.J. Perry, A. Schwenk, Phys. Lett. B 649 (2007) 488.
[6] S.K. Bogner, R.J. Furnstahl, P. Maris, R.J. Perry, A. Schwenk, J.P. Vary, Nucl. Phys. A 801 (2008) 21, arXiv: 0708.3754 [nucl-th].
[7] E. Anderson, S.K. Bogner, R.J. Furnstahl, E.D. Jurgenson, R.J. Perry, A. Schwenk, Phys. Rev. C 77 (2008) 037001, arXiv: 0801.1098 [nucl-th].
[8] S.K. Bogner, R.J. Furnstahl, R.J. Perry, Ann. Phys. 323 (2008) 1478, arXiv: 0708.1602 [nucl-th].
[9] P. Navrátil, G.P. Kamuntavicius, B.R. Barrett, Phys. Rev. C 61 (2000) 044001.
[10] P. Navrátil, B.R. Barrett, Phys. Rev. C 59 (1999) 1906.
[11] P. Navrátil, B.R. Barrett, Phys. Rev. C 57 (1998) 562.
[12] E.D. Jurgenson, S.K. Bogner, R.J. Furnstahl, R.J. Perry, Phys. Rev. C 78 (2008) 014003.
[13] C. Alexandrou, J. Myczkowski, J.W. Negele, Phys. Rev. C 39 (1989) 1076.
[14] D. Van Neck, A.E.L. Dieperink, M. Waroquier, Phys. Rev. C 53 (1996) 2231.
[15] K. Varga, Y. Suzuki, Comput. Phys. Commun. 106 (1997) 157.
[16] E. Anderson, private communication.
[17] E. Epelbaum, A. Nogga, W. Gloeckle, H. Kamada, U.G. Meissner, H. Witala, Phys. Rev. C 66 (2002) 064001.
[18] M. Moshinsky, Y.F. Smirnov, The Harmonic Oscillator in Modern Physics, Harwood Academic Publishers, Amsterdam, 1996.
[19] S. Shlomo, J. Phys. A 16 (1983) 3463–3469.